Biophysical Journal
Article

Biophysical Society

Studies on the X-Ray and Solution Structure of FeoB from *Escherichia coli* BL21

Gregor Hagelueken,[1,*] Jan Hoffmann,[2] Erik Schubert,[1] Fraser G. Duthie,[1] Nicole Florin,[1] Lisa Konrad,[1] Diana Imhof,[3] Elmar Behrmann,[4] Nina Morgner,[2] and Olav Schiemann[1]

[1]Institute for Physical and Theoretical Chemistry,University of Bonn, Bonn, Germany; [2]Institute for Physical and Theoretical Chemistry, Goethe-University Frankfurt, Frankfurt, Germany; [3]Pharmaceutical Chemistry I, Pharmaceutical Institute, University of Bonn, Bonn, Germany; and [4]Research Group Structural Dynamics of Proteins, Center of Advanced European Studes and Research (CAESAR), Bonn, Germany

ABSTRACT The ferrous iron transporter FeoB is an important factor in the iron metabolism of many bacteria. Although several structural studies have been performed on its cytosolic GTPase domain (NFeoB), the full-length structure of FeoB remains elusive. Based on a crystal packing analysis that was performed on crystals of NFeoB, a trimeric structure of the FeoB channel was proposed, where the transport pore runs along the trimer axis. Because this trimer has not been observed in some subsequently solved structures of NFeoB homologs, it remains unclear whether or not the trimer is indeed functionally relevant. Here, pulsed electron-electron double resonance spectroscopy, negative stain electron microscopy, and native mass spectrometry are used to analyze the oligomeric state of different soluble and full-length FeoB constructs. The results show that the full-length protein is predominantly monomeric, whereas dimers and trimers are formed to a small percentage. Furthermore, the solution structure of the switch I region is analyzed by pulsed electron-electron double resonance spectroscopy and a new, to our knowledge, crystal structure of NFeoB from *Escherichia coli* BL21 is presented.

INTRODUCTION

Judged by its mass, iron is the most common element on earth and the fourth most common element in the earth's crust. Iron plays a vital role in many cellular processes, for example electron transport or catalysis. However, the acquisition of iron poses a problem for living cells, because its most abundant ferric form (Fe^{3+}) is almost insoluble under aerobic conditions and at neutral pH. This is especially problematic for organisms such as bacteria, which are confined to very small environments and therefore have to cope with whatever nutrients can be found in their immediate vicinity. As a consequence, bacteria have evolved sophisticated iron scavenging systems, such as iron chelating compounds (siderophores) and dedicated transporters that import the chelated iron into the cell (1). Under anaerobic conditions, the soluble ferrous form of iron (Fe^{2+}) prevails and accordingly, different types of transporters are employed to import this form of iron. A well-known example for such transporters is the 85 kDa ferrous iron transporter FeoB (2). The two-domain protein contains a transmembrane (TM) domain with seven predicted TM helices and a 30 kDa cytoplasmic domain, which has been termed "NFeoB " (as in N-terminal domain of FeoB) (Fig. 1 *A*). NFeoB can again be split into two subdomains, a five-helical bundle and a GTPase domain (3).

Several crystal structures of NFeoB either with or without its nucleotide cofactor have been determined (3–8). These structures have provided valuable structural information, for example concerning the molecular details of the GTPase mechanism (5,6). However, to truly understand the transport mechanism of FeoB, structural information concerning the missing TM domains is needed. In the initial crystal structure of NFeoB (Protein Data Bank (PDB): 3HYT (3)), a trimeric arrangement of the cytosolic domain in the crystal has been observed. It was hypothesized that this arrangement could also be present in the full-length protein, suggesting a transport pore that runs along the trimer axis (3) (Fig. 1 *B*). However, in some subsequently solved crystal structures this arrangement has not been observed (8–10), casting some doubt on the trimer hypothesis. Clearly, only structural information for the whole channel can clarify this matter. Here, the oligomeric states of NFeoB and full-length FeoB are analyzed by a combination of x-ray crystallography, pulsed electron-electron double resonance (PELDOR) spectroscopy, negative stain electron microscopy (EM) and mass spectrometry (MS), providing insights into the oligomeric state of the protein.

Submitted January 20, 2016, and accepted for publication May 6, 2016.

*Correspondence: hagelueken@pc.uni-bonn.de

Editor: David Cafiso.

http://dx.doi.org/10.1016/j.bpj.2016.05.018

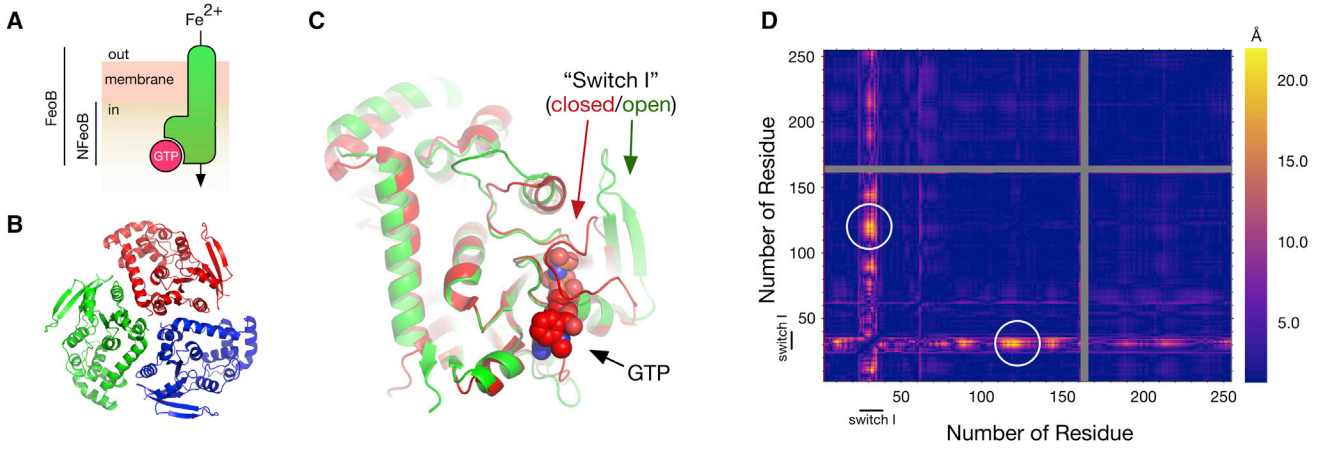

FIGURE 1 Structure of NFeoB from *E. coli* BL21 and selection of labeling sites for PELDOR experiments. (*A*) Sketch of the domain structure of the 85 kDa membrane protein FeoB. The position of the membrane is indicated. NFeoB (30 kDa) is the soluble cytosolic domain of FeoB and contains the GTPase activity. (*B*) The crystallographic trimer of NFeoB from *E. coli* BL21 (this work) is shown as a cartoon model. The three chains are colored differently. (*C*) Structure of an NFeoB monomer. The position of the switch I region (residues 25–40) is marked in its open (*green arrow*, this work) and closed state (*red arrow*, PDB: 3LX5). A black arrow marks the GTP binding pocket with GTP shown as spheres. (*D*) Difference distance matrix (diffDM) of the nucleotide-bound (PDB: 3LX5) and free structures (PDB: 3LX8) of NFeoB. Each position in the diffDM corresponds to a pair of residues in NFeoB. If a conformational change is present between a pair of residues in PDB: 3LX5 and PDB: 3LX8, a difference distance larger than zero results. The magnitude of such difference distances is visualized by a color scale ranging from dark violet (no change) to yellow (largest change, here 22.5 Å). The white circles mark the pair of residues that were used for the experiments below (N32R1-R127R1 (BL21 numbering)). Note that the diffDM is symmetric along its diagonal. The gray areas indicate residues that were not modeled in one of the structures. The switch I region is indicated.

MATERIALS AND METHODS

Protein production and spin labeling

FeoB constructs were cloned, expressed, and purified as previously reported (11). Reconstitution in CHAPSO/DMPC bicelles was performed as previously described (12). To obtain the apo form of NFeoB, any copurified nucleotide was removed by ion exchange chromatography. MTSSL labeling was performed as in (13). The HO4120 spin labeling was performed according to (14). Spin labeling efficiencies of the K1 labeled PELDOR samples were determined by taking 10 μl samples from the PELDOR tubes and recording room temperature X-band cw-EPR spectra on a Bruker (Billerica, MA) EMX-Micro electron paramagnetic resonance (EPR) spectrometer equipped with a 4119HS resonator. The samples were measured at microwave frequency of 9.851 GHz, a resolution of 10 points/Gauss, a microwave power of 2.8 mW, a modulation amplitude of 1 G, a time constant of 0.01 ms, a conversion time of 30.0 ms. The spectra (see Fig. S4 in the Supporting Material) were double integrated using the spectrometer software and compared with HO4120 standards of the same concentration, which were dissolved in PELDOR buffer (100 mM TES pH 7.4, 100 mM NaCl, 0.024% *n*-dodecyl-β-D-maltoside (DDM), 50% deuterated ethylene glycol in D_2O). To get accurate concentrations of the pAcF labeled protein by ultraviolet-visual, the molar extinction coefficient of HO4120 labeled pAcF at 280 nm was experimentally determined (1680 $M^{-1}cm^{-1}$). The labeling degree varied considerably between batches of the same FeoB mutant, so that the labeling degree had to be determined for each individual PELDOR sample. The values for individual samples are given in the results section.

Circular dichroism spectroscopy

Purified NFeoB wild-type (WT) and NFeoBΔCys N32R1 K127R1 were dialyzed against 100 mM NaH_2PO_4/Na_2HPO_4 pH 7.4, diluted to 0.04 mg/ml, and filled into a quartz cuvette with 1 mm path length. Circular dichroism (CD) spectra were recorded on a Jasco-810 spectrometer (Gross-Umstadt, Germany).

Crystallization and structure solution of NFeoB

Purified NFeoB at ~10 mg/ml was used to setup crystallization trials using the JCSG+ Screen (Molecular Dimensions, Newmarket, UK) and 96-well MRC plates (Molecular Dimensions). For each drop, 0.5 μl of protein was mixed with 0.5 μl of reservoir solution. Initial hits were observed in poly(ethylene glycol) (PEG)-based conditions including $MgCl_2$. A stochastic optimization led to final crystallization conditions of 26.9% PEG 8000, 0.39 M $MgCl_2$, 0.1 M Tris-HCl pH8.0. The crystals were grown for several weeks at room temperature before harvesting. Before flash cooling in liquid nitrogen, the crystals were cryoprotected with 35% glycerol. Data were collected at beamline BL14.2 of BESSYII (Berlin, Germany), using a MarMOSAIC 225 charge-coupled device detector. The data were processed using XDS (15) as implemented in XDSAPP (16). See Table 1 for the listing of data collection and processing statistics. The structure of NFeoB was solved using PHASER (17) and PDB: 3I8X (8) as the search model. The PHENIX suite (18) and COOT (19) were used to refine the structure. The geometry of the model was checked and optimized using MOLPROBITY (20).

GTPase assay

The GTPase activity of different FeoB constructs was assayed using a commercial malachite green assay (Bioassay Systems, Hayward, CA), according to (5). Experiments without GTP and/or NFeoB were used as controls and to determine the background of the GTPase assay.

PELDOR spectroscopy

For PELDOR experiments, the spin labeled proteins (typically at 10–25 μM) were dissolved in PELDOR buffer, transferred to a 3 mm quartz Q-band EPR tube and flash cooled in liquid nitrogen. The PELDOR spectra were recorded on a Bruker ELEXSYS E580 pulsed Q-band EPR spectrometer, with a ER 5106QT-2 Q-band resonator. The instrument was equipped with a continuous flow helium cryostat (CF935) and temperature control

TABLE 1 Data Collection and Refinement Statistics

	NFeoB
Data Collection	
Wavelength (Å)	0.9085
Resolution range (Å)	48.12–3.16 (3.272–3.16)
Space group	P 6_3
Unit cell (Å)	166.7 166.7 65.6 90 90 120
Total reflections	135770 (12380)
Unique reflections	18052 (1753)
Multiplicity	7.5 (7.1)
Completeness (%)	99.6 (96.3)
Mean I/sigma (I)	9.11 (1.39)
Wilson B-factor (Å^2)	71.34
R-merge	0.2328 (1.384)
R-meas	0.2501
CC1/2	0.992 (0.362)
CC*	0.998 (0.729)
Refinement	
R-work	0.207 (0.341)
R-free	0.238 (0.360)
Number of nonhydrogen atoms	3886
Protein residues	509
RMS (bonds)	0.007
RMS (angles)	1.5
Ramachandran favored (%)	97
Ramachandran outliers (%)	0.6
Clashscore	7.01
Molprobity Score	1.77
Average B-factor (Å^2)	75.1

Values in parentheses represent values for the shell of highest resolution.

system (ITC 502), both from Oxford instruments (Abingdon, UK). The second microwave frequency was coupled into the microwave bridge using a commercially available setup from Bruker. All pulses were amplified via a pulsed traveling wave tube amplifier. PELDOR experiments were performed with the pulse sequence $\pi/2(\nu A)$-$\tau 1$-$\pi(\nu A)$-$(\tau 1+t)$-$\pi(\nu B)$-$(\tau 2-t)$-$\pi(\nu A)$-$\tau 2$-echo. The detection pulses (νA) were set to 12 ns for the $\pi/2$ and 24 ns for the π pulses and applied at a frequency 80 MHz lower than the resonance frequency of the resonator. The pulse amplitudes were chosen to optimize the refocused echo. The $\pi/2$-pulse was phase-cycled to eliminate receiver offsets. The pump pulse (νB) was set at the resonance frequency of the resonator and its optimal length (typically 12–16 ns) was determined using a transient nutation experiment for each sample. The field was adjusted such that the pump pulse is applied to the maximum of the nitroxide spectrum. The pulse amplitude was optimized to maximize the inversion of a Hahn-echo at the pump frequency. All PELDOR spectra were recorded at 50 K with an experiment repetition time of 1 ms, a video amplifier bandwidth of 20 MHz and an amplifier gain of 42 dB. $\tau 1$ was set to 260 ns and the maximum of $\tau 2$ was set to values ranging from 1000 to 5000 ns. Deuterium modulation was suppressed by addition of 8 spectra of variable $\tau 1$ with a $\Delta\tau 1$ of 16 ns. The obtained time traces were divided by a monoexponential decay to eliminate intermolecular contributions and renormalized. Distance distributions were obtained from the background corrected data by using the program DeerAnalysis2015 developed by Gunnar Jeschke (21). The PyMOL (www.pymol.org) plugin mtsslWizard was used to predict distance distributions (22).

Negative stain EM and estimation of size distribution

Full-length FeoB (0.7 mg/ml) in 3× critical micelle concentration (CMC) DDM buffer (100 mM TES pH 8.0, 150 mM NaCl, 0.024% DDM) was freshly diluted in 1.5× CMC DDM buffer (100 mM TES pH 8.0, 100 mM NaCl, 0.012% DDM), and 3.5 μl samples applied to freshly glow-discharged holey carbon grids covered with an additional thin carbon support film (R2/1 + 5nm carbon, Quantifoil, Germany). Grids were washed twice with detergent-free buffer to disrupt empty DDM micelles, and stained using uranyl formate (0.75% w/v) solution adjusted to pH 7.5 with sodium hydroxide. Electron micrographs were collected under minimal-dose conditions on a Jeol (Freising, Germany) JEM2200 equipped with a TVIPS TemCam-F416 CMOS camera at a nominal magnification of 40,000. Micrographs were collected at an acceleration voltage of 200 kV with a defocus range of -1 to -5 μm. The pixel-size at the object plane corresponds to 2.9 Å/pixel. Defocus estimation was performed using CTER (23), and micrographs were preselected based on calculated defocus and astigmatism values. Strong heterogeneity precluded particle classification procedures. Thus, the size distribution of individual particle images was estimated from line histograms after phase flipping to restore the actual object image.

MS

For laser-induced liquid bead ion desorption-mass spectrometry (LILBID-MS) measurements the protein was buffer exchanged to 20 mM Tris with 0.03% DDM at pH 8.0, directly before the measurement. The buffer exchange took place in desalting columns (Zeba Micro Spin Desalting Columns, article number 89887) from Thermo Scientific (Waltham, MA) (7 kDa cut-off). Alternatively, the sample was spun down at 12.000 g for 10 min and the supernatant was washed twice in 20 mM NH_4HCO_3 with 0.03% DDM at pH 8. The washing took place in centrifugal filters (Amicon Ultra-0.5 mL, article number UFC503024) from Merck Millipore (Darmstadt, Germany) (30 kDa cut-off). In each case 5 μL of the sample was used per measurement. A piezo-driven droplet generator was used to generate LILBID-MS droplets (MD-K-130 by Microdrop Technologies GmbH, Norderstedt, Germany). This generator produces droplets of 50 μm diameter with a frequency of 10 Hz. The droplets were transferred to vacuum and irradiated by an infrared (IR) laser at 2.94 μm, a vibrational absorption wavelength of water, which leads to the explosive expansion of the droplet. The released ions are accelerated by a pulsed electric field and the mass of the ions is analyzed by a homebuilt reflectron time-of-flight setup. The LILBID instrument was run at standard settings (24). For each spectrum, data from several hundred up to a thousand droplets were averaged. Data processing was done using the software *Mass*ign (25).

RESULTS

X-ray crystal structure of NFeoB from *Escherichia coli* BL21

NFeoB from *E. coli* BL21 was cloned, expressed, and purified as previously reported (11). When purified from *E. coli* BL21, the protein contained a nucleotide, presumably GTP, which was removed during ion exchange chromatography (11). The purified protein crystallized in space group $P6_3$ at a concentration of ~10 mg/ml in 26.9% PEG 8000, 0.39 M $MgCl_2$, 0.1 M Tris-HCl pH 8.0. The structure was solved at a resolution of 3.16 Å by molecular replacement. The structure of monomeric GDP-bound NFeoB was used as a search model (PDB: 3I8X (8)). Fig. 1. *B* and *C*, show the overall structure of the protein. As observed previously, NFeoB forms as a trimer in the crystal. The refined structure aligns with a root mean-square deviation (r.m.s.d.) of 0.38 Å (212 Cα-Atoms) with the search model. Presumably due to

the absence of a nucleotide, the "switch I" region is observed in its opened conformation. Data collection and refinement statistics are compiled in Table 1.

PELDOR studies on the switch I region of NFeoB

The way in which GTP/GDP regulates the transport activity of FeoB is unknown. Presumably, binding of the cofactor induces conformational changes, triggering the gating mechanism of FeoB. It has also been suggested that GTP hydrolysis may be used to power an active transport mechanism (5). To analyze the conformational changes in NFeoB upon GTP binding, a difference distance matrix (diffDM) between nucleotide-free and bound structures (5) was calculated using the program mtsslWizard (22,26). See Fig. 1 *D*, which illustrates that the largest conformational changes upon nucleotide binding occur in the switch I region (residues 25–40), directly adjacent to the GTP-binding pocket. A large conformational change of ~20 Å occurs between the Cβ atoms of residues N32 and K127 (Fig. 1, *C* and *D*). PELDOR or DEER distance measurements in combination with site-directed spin labeling (27) are a possible way to determine, whether this conformational change also occurs in solution. In both crystal structures (closed and open), the two residues are located at the molecular surface and are therefore well suited for the introduction of spin labels. For the site-specific incorporation of the two labels at these sites, the five indigenous cysteines of NFeoB were removed and two new cysteines were introduced at positions N32 and K127. The modified protein (NFeoBΔCys N32C K127C) expressed at similar levels as the WT protein and was capable of binding GTP (Fig. S1). The CD spectrum of the mutant was virtually identical to that of WT NFeoB (Fig. S2). MTSSL (28) spin labels were introduced and the N32R1-K127R1 distance (MTSSL modified Cys are commonly termed R1) was determined for the apo protein using Q-band PELDOR spectroscopy at a protein concentration of 25 μM (Fig. 2 *A*, *black line*). Note that equimolar (with respect to the cofactor) amounts of $MgCl_2$ were included in all measurements presented below. The resulting PELDOR time trace showed a modulation depth of 40% as commonly found for a doubly spin labeled protein (29). The DeerAnalysis software package was used to calculate the underlying distance distribution (Fig. 2 *B*, *black line*) (21). An unimodal distance distribution with an average distance of ~40 Å and a distribution width of ~12 Å was observed.

In comparison, mtsslWizard predicts the distance distributions that are shown as green and red shapes (Fig. 3 *B*) for the open and closed states of the N32R1-K127R1 mutant, respectively. Considering the error of in silico spin labeling programs of ± 3 Å (22,30,31), the prediction made by mtsslWizard for the open state provides a good fit to the experimental distance distribution. Therefore, it seems safe to assume that apo-NFeoB adopts the open conformation in solution. Addition of GTP or GDP (500 μM, 20-fold molar excess) led only to small changes in the width of the distribution and an increase of a very small peak at 20 Å that might correspond to the closed form of the switch I loop (Fig. 2 *B*). A slightly stronger increase of the 20 Å peak was observed for the nonhydrolysable GTP analog GMPPNP at 100-fold molar excess (Fig. 2, *A* and *B*, *purple curves*). It has been shown that potassium ions can strongly accelerate the GTPase activity of NFeoB (5). To test if KCl has an influence on the conformation of the switch I loop, a PELDOR experiment with 100-fold molar excess of GMPPNP and 100 mM KCl was performed. However, the resulting PELDOR time trace and corresponding distance distribution did not differ significantly from the one recorded without KCl (*purple* and *red curves* in Fig. 2, *A* and *B*). To exclude that removal of the cysteines or the addition of the

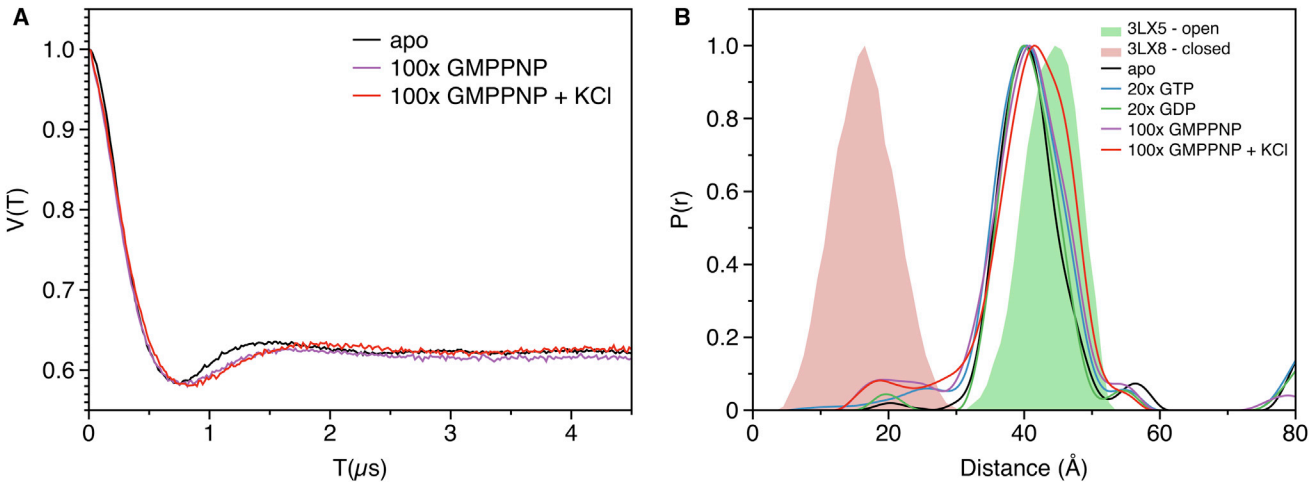

FIGURE 2 PELDOR spectroscopy on the switch I region of NFeoB. (*A*) Q-band PELDOR time traces for NFeoB measured under different conditions, as indicated in the legend. The data sets were processed with the series option of DeerAnalysis. (*B*) Distance distributions from the time traces in (*A*), as calculated by DeerAnalysis (21). MtsslWizard predictions for the open- (*green shape*) and closed (*red shape*) NFeoB structures are shown.

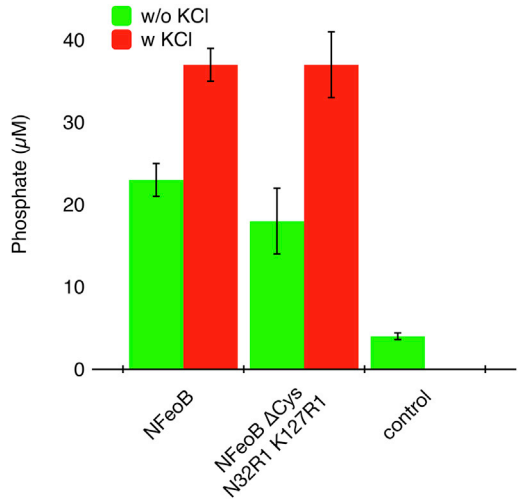

FIGURE 3 GTPase activity of NFeoB constructs. Error bars indicate the standard deviation calculated from a triplicate of measurements. To see this figure in color, go online.

spin label induced an artificial "open-locked state" of the switch I region in NFeoBΔCys N32R1 K127R1, its activity was analyzed using a malachite-green based GTP hydrolysis assay. The results shown in Fig. 3 confirm that the NFeoBΔCys N32R1 K127R1 mutant has the same activity as the WT protein. Furthermore, the activation by KCl was observed for both WT and mutant NFeoB.

Oligomeric state of FeoB analyzed by PELDOR spectroscopy

Although NFeoB commonly crystallizes as a trimer (Fig. 1 *B*), it is to date unclear, whether this crystallographically observed trimer is of any functional relevance. To investigate the solution structures of NFeoB and full-length FeoB with PELDOR spectroscopy, two solvent accessible labeling sites K127 and R152 were selected based on the structure of the NFeoB trimer (Fig. 1 *B*). The unnatural amino acid para-acetylphenylalanin (pAcF) was introduced at positon 127 of NFeoB and 127 or 152 of full-length FeoB. The pAcF residue was then labeled with HO4120, producing the K1 spin label (32,33). This strategy was used because full-length FeoB from *E. coli* BL21 contains 12 cysteines, which would all have to be replaced before site-directed spin labeling with R1 could have been applied. On average, the efficiency of the labeling procedure was 52 ± 15%.

To investigate if PELDOR spectroscopy can provide evidence for the crystallographic NFeoB trimer in solution, a sample with 25 μM NFeoB K127K1 was prepared. The resulting PELDOR time trace could be fitted with a homogenous three-dimensional (3D) background (Fig. 4 *A*). In contrast, increasing the NFeoB K127K1 concentration to 516 μM, resulted in a PELDOR time trace that could not be completely fitted with a 3D background function (Fig. 4 *A*). Dividing the 516 μM time trace by a homogenous 3D background left a modulation depth of ~0.05. Analyzing this with DeerAnalysis yielded a very broad distance distribution ($\Delta r = 45$ Å) centered around 40 Å (Fig. 4 *B*) (21). It appears that at this relatively high concentration, the NFeoB K127K1 monomers are indeed physically interacting with each other. For the crystallographic trimer (Fig. 1 *B*), the mtsslWizard software (22) predicts a distance distribution centered at 25 Å (Fig. 4 *B*, *green shade*). The experimental distribution indeed contains such distances but is much broader. Thus, the experimentally observed interactions seem to be rather unspecific.

It is possible that the TM domain of FeoB is needed to stabilize the trimeric arrangement in solution. Therefore, as a next step, PELDOR experiments on DDM solubilized full-length FeoB K127K1 and FeoB K152K1 were conducted. Both mutants yielded time traces that clearly deviated from a homogenous 3D background. Dividing this background left an intraoligomer contribution with a modulation depth of 0.03 and 0.05 for mutants K127K1 and R152K1, respectively (Fig. 4, *C* and *E*). It is well established that information about the number of interacting spins in a particular sample is encoded in the modulation depth of the PELDOR time trace (29). For example, assuming a well-optimized PELDOR experiment at Q-band, a modulation depth of 0.4 is expected for a biradical and 0.64 for a triradical (29,34). However, the modulation depth is also strongly dependent on the labeling degree, which can vary significantly between different samples. We therefore determined the labeling degree for each particular PELDOR sample after the PELDOR experiment had been completed. As a control experiment, a pair of K1 labels was introduced into NFeoB at positions K127 and R152. The labeling efficiency of this sample was determined (52%) and a PELDOR time trace was recorded, revealing a modulation depth of 0.14 (see Fig. 4 *G*). This value fits reasonably well to the expected modulation depth for a biradical at 52% labeling efficiency (see Fig. 4 *H*). Next, the labeling efficiencies of the actual full-length FeoB K127K1 and R152K1 PELDOR samples were determined (73% and 32% labeling efficiency, respectively). For both samples, Fig. 4 *H* reveals a large difference between the experimentally observed modulation depths and the expected modulation depths for a triradical. To verify that the detergent environment does not disturb the oligomeric state of FeoB, the FeoBR152K1 sample was reconstituted in CHAPSO/DMPC bicelles. The resulting PELDOR time trace was very similar to the DDM sample and, if anything, revealed an even lower modulation depth (see Fig. 4 *E*). For both FeoB K127K1 and R152K1, data processing with DeerAnalysis led to broad distance distributions centered around 18 Å (Fig. 4, *D* and *F*). Minor features at distances predicted for the crystallographic trimer were observed (trimer structure shown in Fig. 1 *B* was used to predict distances with mtsslWizard). It should be noted that due to the very low modulation depths and the absence of prominent oscillations

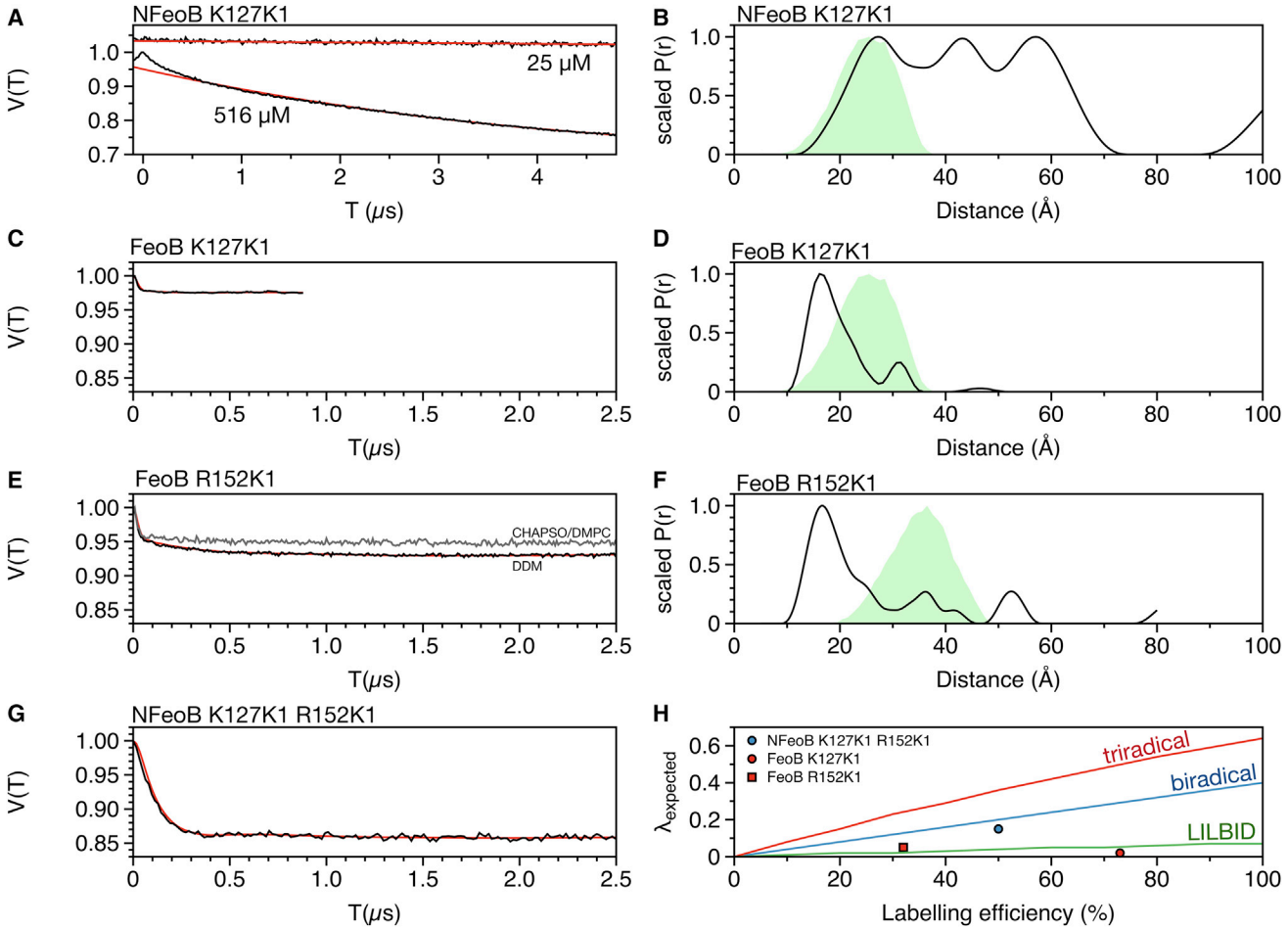

FIGURE 4 PELDOR experiments on spin labeled FeoB constructs. (*A*) PELDOR time traces of singly spin labeled NFeoB K127K1 at 25 and 516 μM protein concentration. The experimental data are shown as black lines, the fitted background functions as red lines. (*B*) The distance distribution for the 516 μM NFeoB sample produced by DeerAnalysis is shown as a black line. The predicted distance distribution for an NFeoB K127K1 trimer (Fig. 1 *B*) is shown as a green shade. (*C*) Background corrected PELDOR time trace of singly spin labeled full length FeoB K127K1 (*black*, experiment; *red*, fit). (*D*) The distance distribution for the FeoB K127K1 sample is shown as a black line. The predicted distance distribution for an NFeoB K127K1 trimer (Fig. 1 *B*) is shown as a green shade. (*E*) Background corrected PELDOR time trace of singly spin labeled full-length FeoB R152K1 (*black*, experiment; *red*, fit; *gray*, experiment in CHAPSO/DMPC bicelles). (*F*) The distance distribution for the FeoB R152K1 sample (in DDM) is shown as a black line. The predicted distance distribution for an NFeoB R152K1 trimer (Fig. 1 *B*) is shown as a green shade. (*G*) Background corrected PELDOR time trace of a doubly labeled NFeoB K127K1 R152K1 sample (*black*, experiment; *red*, fit). (*H*) Plots of $\lambda_{expected}$ over % labeling efficiency for bi- and triradicals (*blue* and *red curves*, respectively). The expected modulation depth was calculated using the formula $\lambda_{expected} = 1\text{-}(1\text{-}a^{*}\lambda_B)^{(n-1)}$. The formula is based on (29). Here, the λ_B parameter was scaled by the labeling efficiency a, which runs from 0 to 1. The labeling efficiencies and modulation depths for the samples shown in (*C*), (*E*), and (*G*) are plotted as indicated in the legend. The green curve represents $\lambda_{expected}$ for a (8.5:1:0.5) mixture of monomers/dimers/trimers as determined by LILBID-MS (see below). The curve was calculated according to (29). To see this figure in color, go online.

in the time traces, the features of the produced distance distributions should be interpreted with care. Summing up, the PELDOR results do not agree well with a defined trimeric state of full-length FeoB in detergent solutions. However, small amounts of multimers that are perhaps functionally relevant, are clearly present in our samples.

Oligomeric state of FeoB analyzed by LILBID-MS and negative stain EM

LILBID-MS was used to investigate the oligomerization state of FeoB with an orthogonal method. LILBID-MS can determine native masses of noncovalently bound macromolecular complexes (e.g., oligomers of a protein) in DDM solutions (35). For a particular sample that contains a distribution of oligomeric states of the same protein, the LILBID-MS mass spectrum can be quantitatively analyzed. Full-length FeoB (WT) at a concentration of 150 μM was subjected to the analysis and the resulting mass spectrum is shown in Fig. 5 *A*.

The LILBID-MS spectrum in Fig. 5 *A* was analyzed using the *Mass*ign software package (25) and showed strong peaks at the expected masses for the singly and doubly charged species of the FeoB monomer (85 kDa, *red* M in Fig. 5).

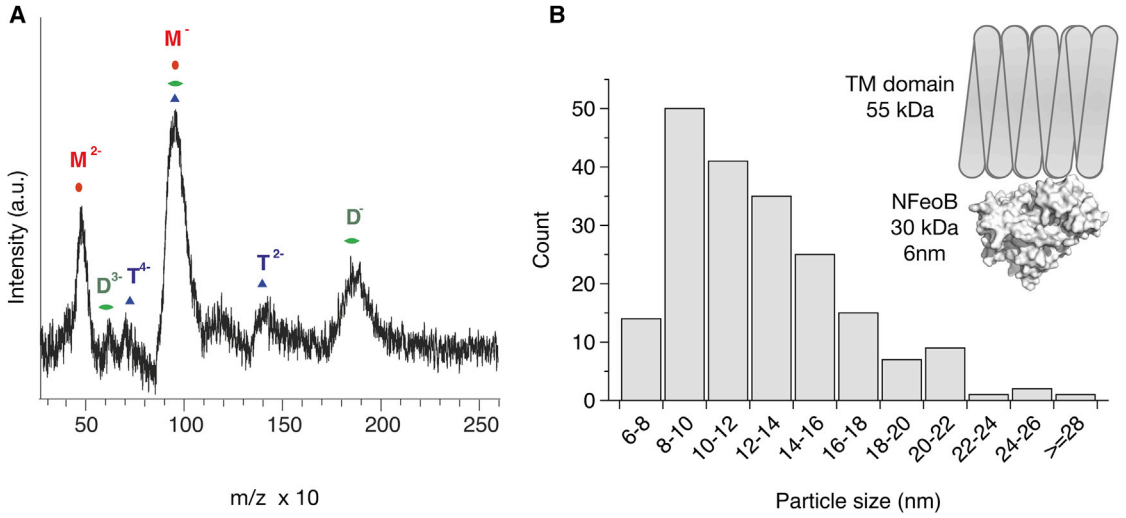

FIGURE 5 LILBID-MS and negative stain EM size distribution of full length FeoB samples. (*A*) The mass spectrum is shown as a black line. Major peaks are indicated by M, D, and T for monomer, dimer, and trimer, respectively. Numbers in superscript indicate the charge state of the particles. (*B*) Particle size distribution determined from negative stain EM micrographs of full-length FeoB. A representative raw micrograph is shown in Fig. S3. The inset illustrates the size of full-length FeoB in comparison to the crystal structure of NFeoB, which has a diameter of up to ~6 nm. To see this figure in color, go online.

Note that the broadness of the peaks is due to the detergent micelle. Clear but less intense peaks were also identified for dimeric FeoB (Fig. 5, *green* D) and weak evidence for a trimeric species was found (Fig. 5, *blue* T). To cross-validate the LILBID-MS and PELDOR results, the relative ratios of the three species were estimated (~8.5:1:0.5) and the expected PELDOR modulation depth of such a mixture was calculated for different labeling efficiencies (29). The predicted modulation depths fit very well to the PELDOR results (Fig. 4 *H*, *green curve*). As an additional control, we recorded negative stain EM micrographs of our FeoB preparations and determined a size distribution of the observed particles (Figs. 5 *B* and S3). The most abundant particles have a size of 8–10 nm and may be interpreted as a side-on view of a FeoB monomer. We neither observed a significant number of symmetrical particles, nor a significant amount of larger dimension particles as would be expected for a sample consisting of a defined trimeric species.

DISCUSSION

Crystal structures of NFeoB have revealed the opened and closed states of the switch I region (5,6). A detailed biochemical study showed that the GTPase activity of NFeoB increases 20-fold when K^+ ions are added to the reaction buffer. This effect was attributed to a coordination of the K^+ ion by both the nucleotide and the switch I loop (5). The PELDOR results above confirm that also in solution, the switch I loop can indeed occupy either the open or closed position (Fig. 2). However, it is surprising that even with the addition of 100× excesses of GMPPNP, Mg^{2+}, and K^+, only a small fraction of the molecules (~5%) are observed in the closed state. It is of course possible that the addition of the spin label leads to an artificial stabilization of the switch I loop in the opened state. However, the observed equal activities of WT and spin labeled protein, together with an equally strong activation by K^+ ions seem to contradict this notion (Fig. 3). Note that the kinetics of wild-type and mutant reactions were not analyzed and might differ. Assuming that the spin labels do not distort the dynamics of the switch-I loop, one could speculate that in the full-length protein, the closing of the switch I loop induces a conformational change of the whole channel, which also leads to its own stabilization in the closed conformation. Clearly, this hypothesis needs to be proven by further experiments.

It is a commonly met question, whether or not a crystallographically observed multimer is of any functional relevance. Different theoretical and experimental methods can be applied to solve this question. The PISA server (36) analyses crystal-packing interactions to predict the most probable oligomeric state of the protein in solution. In the case of NFeoB (Fig. 1), the server does not give a conclusive answer, because different results are obtained for different NFeoB input structures. Probably the most straightforward experimental way to analyze the oligomeric state of a protein construct are gelfiltration experiments. We and others have previously performed this experiment for NFeoB and no indication of a multimeric state has been observed for WT NFeoB constructs (8,11). However, because NFeoB lacks a large proportion of the full-length protein (Fig. 1 *A*), the multimer may destabilize and only form at high concentrations. Gelfiltration is not the method of choice for such weak complexes, because the different species are separated and significantly diluted during the gelfiltration run. PELDOR distance measurements have been shown to be a

suitable method to validate crystallographic multimers in solution (37). Here, PELDOR spectroscopy experiments on singly spin labeled NFeoB revealed that the protein is monomeric at low concentrations (25 μM) but that small amounts of oligomers (~5%) are formed at higher concentrations (516 μM, Fig. 4 *A*). An analysis of the 516 μM PELDOR time trace with DeerAnalysis (21) revealed a very broad distribution of interspin distances (Fig. 4 *B*). Indeed, the experimental distribution contains the distances that are predicted from the crystallographic trimer (Figs. 1 *B* and 4 *B*). However, the trimer only explains a small fraction of the experimental distance distribution. This may be interpreted as a rather unspecific interaction of the NFeoB monomers in the PELDOR sample. Apparently, the nascent crystal lattice selectively incorporates the observed crystallographic trimer.

It is possible that the TM domain of FeoB is needed to stabilize a trimeric structure of the channel in solution. In an earlier study we have conducted gelfiltration experiments on DDM solubilized full-length FeoB (11). Judged by its elution volume (Superdex 200 column), the protein appeared to form multimers. However, as already discussed at the time (11), due to the presence of the detergent micelle and the sensitivity of this sizing method to the overall shape of the protein-detergent complex, size determinations of membrane proteins by gelfiltrations are error prone. To get a more precise insight into the detergent structure of FeoB, PELDOR experiments on singly spin labeled full-length FeoB mutants were performed in this work (Fig. 4). PELDOR is not affected by the size of the detergent micelle or the shape of the molecule. Furthermore, it is well established that the modulation depths of the PELDOR time traces contain information about the oligomeric state of the underlying spin system (29). Taking the labeling degree of the PELDOR samples carefully into account, neither the observed modulation depths nor the calculated PELDOR distance distributions agree well with a defined trimeric state of the FeoB channel in detergent solution or in the artificial membrane environment of CHAPSO/DMPC bicelles (Fig. 4). The LILBID-MS and negative-stain EM results confirm the PELDOR results (Fig. 5). LILBID-MS revealed a distribution of monomers/dimers/trimers with an estimated ratio of ~8.5:1:0.5. The expected PELDOR modulation depth for such a mixture was calculated and fits very well to the experimentally observed values (Fig. 4 *H*). Also, a recent atomic force microscopy study on FeoB from *Pseudomonas aeruginosa* revealed a large amount of monomers in FeoB samples, whereas peaks interpreted as trimers and hexamers were found to a smaller extent (38). Taken together, it appears that both NFeoB and full-length FeoB are mostly monomeric in solution, while oligomers are formed to a small extent. This explains the earlier observation that the rotational correlation time of FeoB K127K1 determined by cw-X-band EPR spectroscopy is larger than expected for the monomeric protein (11). Note that we cannot exclude that the functionally relevant form of the FeoB channel is found among the small percentage of observed oligomers. An equilibrium between the different states might even be important for the function of FeoB. Until a crystal structure of the complete channel has been solved and the nature of the transport pore tested, e.g., by mutational analysis, it will remain very difficult to unravel the biologically relevant structure of this channel.

CONCLUSIONS

The PELDOR results on the switch I region of NFeoB provide strong evidence that the crystallographically observed open and closed forms of the switch I region also exist in solution. Surprisingly, the closed form is only formed to a small percentage, even at high concentrations of GMPPNP. The PELDOR, LILBID-MS, and EM results on full-length FeoB do not support the crystallographic trimer as the predominant structure of the FeoB channel in detergent or CHAPSO/DMPC bicelles. However, small amounts of FeoB oligomers were clearly observed and it cannot be excluded that the functional form of the channel can be found among these multimers.

SUPPORTING MATERIAL

Four figures are available at http://www.biophysj.org/biophysj/supplemental/S0006-3495(16)30300-9.

AUTHOR CONTRIBUTIONS

G.H., D.I., and O.S. designed research; G.H., J.H. E.S., F.G.D, N.F., L.K., and E.B. performed research; N.M. J.H., and E.B. contributed analytic tools; G.H., O.S., N.M., J.H., and E.B. analyzed data; G.H., N.M., J.H., E.B., and O.S. wrote the article.

ACKNOWLEDGMENTS

G.H., O.S., and D.I. thank the German Research Foundation (DFG) for funding this project within the Collaborative Research Center (SFB) 813. G.H. acknowledges beamtime and assistance at BL14.2 of BESSY II. N.M. acknowledges support by the European Research Council under the European Union's Seventh Framework Programme (FP7/2007-2013)/ERC Grant agreement No. 337567. E.B. holds a Freigeist-Fellowship from the Volkswagen Foundation and acknowledges continuous support from the Caesar Foundation.

REFERENCES

1. Neilands, J. B. 1995. Siderophores: structure and function of microbial iron transport compounds. *J. Biol. Chem.* 270:26723–26726.
2. Kammler, M., C. Schön, and K. Hantke. 1993. Characterization of the ferrous iron uptake system of *Escherichia coli*. *J. Bacteriol.* 175:6212–6219.
3. Guilfoyle, A., M. J. Maher, …, M. Jormakka. 2009. Structural basis of GDP release and gating in G protein coupled Fe2+ transport. *EMBO J.* 28:2677–2685.

4. Hung, K.-W., J.-Y. Tsai, …, T.-H. Huang. 2012. Crystal structure of the *Klebsiella pneumoniae* NFeoB/FeoC complex and roles of FeoC in regulation of Fe2+ transport by the bacterial Feo system. *J. Bacteriol.* 194:6518–6526.
5. Ash, M.-R., A. Guilfoyle, …, M. Jormakka. 2010. Potassium-activated GTPase reaction in the G Protein-coupled ferrous iron transporter B. *J. Biol. Chem.* 285:14594–14602.
6. Ash, M.-R., M. J. Maher, …, M. Jormakka. 2011. A suite of Switch I and Switch II mutant structures from the G-protein domain of FeoB. *Acta Crystallogr. D Biol. Crystallogr.* 67:973–980.
7. Deshpande, C. N., A. P. McGrath, …, M. Jormakka. 2013. Structure of an atypical FeoB G-domain reveals a putative domain-swapped dimer. *Acta Crystallogr. Sect. F Struct. Biol. Cryst. Commun.* 69:399–404.
8. Petermann, N., G. Hansen, …, R. Hilgenfeld. 2010. Structure of the GTPase and GDI domains of FeoB, the ferrous iron transporter of *Legionella pneumophila*. *FEBS Lett.* 584:733–738.
9. Köster, S., M. Wehner, …, O. Yildiz. 2009. Structure and function of the FeoB G-domain from *Methanococcus jannaschii*. *J. Mol. Biol.* 392:405–419.
10. Hattori, M., Y. Jin, …, O. Nureki. 2009. Structural basis of novel interactions between the small-GTPase and GDI-like domains in prokaryotic FeoB iron transporter. *Structure*. 17:1345–1355.
11. Hagelueken, G., F. G. Duthie, …, O. Schiemann. 2015. Expression, purification and spin labelling of the ferrous iron transporter FeoB from *Escherichia coli* BL21 for EPR studies. *Protein Expr. Purif.* 114:30–36.
12. Ward, R., C. Pliotas, …, O. Schiemann. 2014. Probing the structure of the mechanosensitive channel of small conductance in lipid bilayers with pulsed electron-electron double resonance. *Biophys. J.* 106: 834–842.
13. Hagelueken, G., W. J. Ingledew, …, J. H. Naismith. 2009. PELDOR spectroscopy distance fingerprinting of the octameric outer-membrane protein Wza from *Escherichia coli*. *Angew. Chem. Int. Ed. Engl.* 48:2904–2906.
14. Evans, E. G. B., and G. L. Millhauser. 2015. Genetic incorporation of the unnatural amino acid *p*-acetyl phenylalanine into proteins for site-directed spin labeling. *Methods Enzymol.* 563:503–527.
15. Kabsch, W. 1988. Automatic-indexing of rotation diffraction patterns. *J. Appl. Cryst.* 21:67–71.
16. Krug, M., M. S. Weiss, …, U. Mueller. 2012. XDSAPP: a graphical user interface for the convenient processing of diffraction data using XDS. *J. Appl. Cryst.* 45:568–572.
17. McCoy, A. J., R. W. Grosse-Kunstleve, …, R. J. Read. 2007. Phaser crystallographic software. *J. Appl. Cryst.* 40:658–674.
18. Adams, P. D., R. W. Grosse-Kunstleve, …, T. C. Terwilliger. 2002. PHENIX: building new software for automated crystallographic structure determination. *Acta Crystallogr. D Biol. Crystallogr.* 58:1948–1954.
19. Emsley, P., and K. Cowtan. 2004. Coot: model-building tools for molecular graphics. *Acta Crystallogr. D Biol. Crystallogr.* 60:2126–2132.
20. Chen, V. B., W. B. Arendall, 3rd, …, D. C. Richardson. 2010. MolProbity: all-atom structure validation for macromolecular crystallography. *Acta Crystallogr. D Biol. Crystallogr.* 66:12–21.
21. Jeschke, G., V. Chechik, …, A. Godt. 2006. DeerAnalysis2006—a comprehensive software package for analyzing pulsed ELDOR data. *Appl. Magn. Reson.* 30:473–498.
22. Hagelueken, G., R. Ward, …, O. Schiemann. 2012. MtsslWizard: in silico spin-labeling and generation of distance distributions in PyMOL. *Appl. Magn. Reson.* 42:377–391.
23. Penczek, P. A., J. Fang, …, C. M. T. Spahn. 2014. CTER-rapid estimation of CTF parameters with error assessment. *Ultramicroscopy.* 140:9–19.
24. Morgner, N., H. D. Barth, and B. Brutschy. 2006. A new way to detect noncovalently bonded complexes of biomolecules from liquid microdroplets by laser mass spectrometry. *Aust. J. Chem.* 59:109–114.
25. Morgner, N., and C. V. Robinson. 2012. Massign: an assignment strategy for maximizing information from the mass spectra of heterogeneous protein assemblies. *Anal. Chem.* 84:2939–2948.
26. Hagelueken, G., D. Abdullin, and O. Schiemann. 2015. mtsslSuite: probing biomolecular conformation by spin-labeling studies. *Methods Enzymol.* 563:595–622.
27. Jeschke, G. 2012. DEER distance measurements on proteins. *Annu. Rev. Phys. Chem.* 63:419–446.
28. Berliner, L. J., J. Grunwald, …, K. Hideg. 1982. A novel reversible thiol-specific spin label: papain active site labeling and inhibition. *Anal. Biochem.* 119:450–455.
29. Bode, B. E., D. Margraf, …, O. Schiemann. 2007. Counting the monomers in nanometer-sized oligomers by pulsed electron-electron double resonance. *J. Am. Chem. Soc.* 129:6736–6745.
30. Jeschke, G. 2013. Conformational dynamics and distribution of nitroxide spin labels. *Prog. Nucl. Magn. Reson. Spectrosc.* 72:42–60.
31. Alexander, N. S., R. A. Stein, …, J. Meiler. 2013. RosettaEPR: rotamer library for spin label structure and dynamics. *PLoS One.* 8:e72851.
32. Young, T. S., I. Ahmad, …, P. G. Schultz. 2010. An enhanced system for unnatural amino acid mutagenesis in *E. coli*. *J. Mol. Biol.* 395:361–374.
33. Fleissner, M. R., E. M. Brustad, …, W. L. Hubbell. 2009. Site-directed spin labeling of a genetically encoded unnatural amino acid. *Proc. Natl. Acad. Sci. USA.* 106:21637–21642.
34. Polyhach, Y., E. Bordignon, …, G. Jeschke. 2012. High sensitivity and versatility of the DEER experiment on nitroxide radical pairs at Q-band frequencies. *Phys. Chem. Chem. Phys.* 14:10762–10773.
35. Morgner, N., and C. V. Robinson. 2012. Linking structural change with functional regulation-insights from mass spectrometry. *Curr. Opin. Struct. Biol.* 22:44–51.
36. Krissinel, E. 2010. Crystal contacts as nature's docking solutions. *J. Comput. Chem.* 31:133–143.
37. Kerry, P. S., H. L. Turkington, …, B. E. Bode. 2014. Analysis of influenza A virus NS1 dimer interfaces in solution by pulse EPR distance measurements. *J. Phys. Chem. B.* 118:10882–10888.
38. Seyedmohammad, S., N. A. Fuentealba, …, H. Venter. 2016. Structural model of FeoB, the iron transporter from *Pseudomonas aeruginosa*, predicts a cysteine lined, GTP-gated pore. *Biosci. Rep.* 36:e00322.

Biophysical Journal, Volume *110*

Supplemental Information

Studies on the X-Ray and Solution Structure of FeoB from *Escherichia coli* BL21

Gregor Hagelueken, Jan Hoffmann, Erik Schubert, Fraser G. Duthie, Nicole Florin, Lisa Konrad, Diana Imhof, Elmar Behrmann, Nina Morgner, and Olav Schiemann

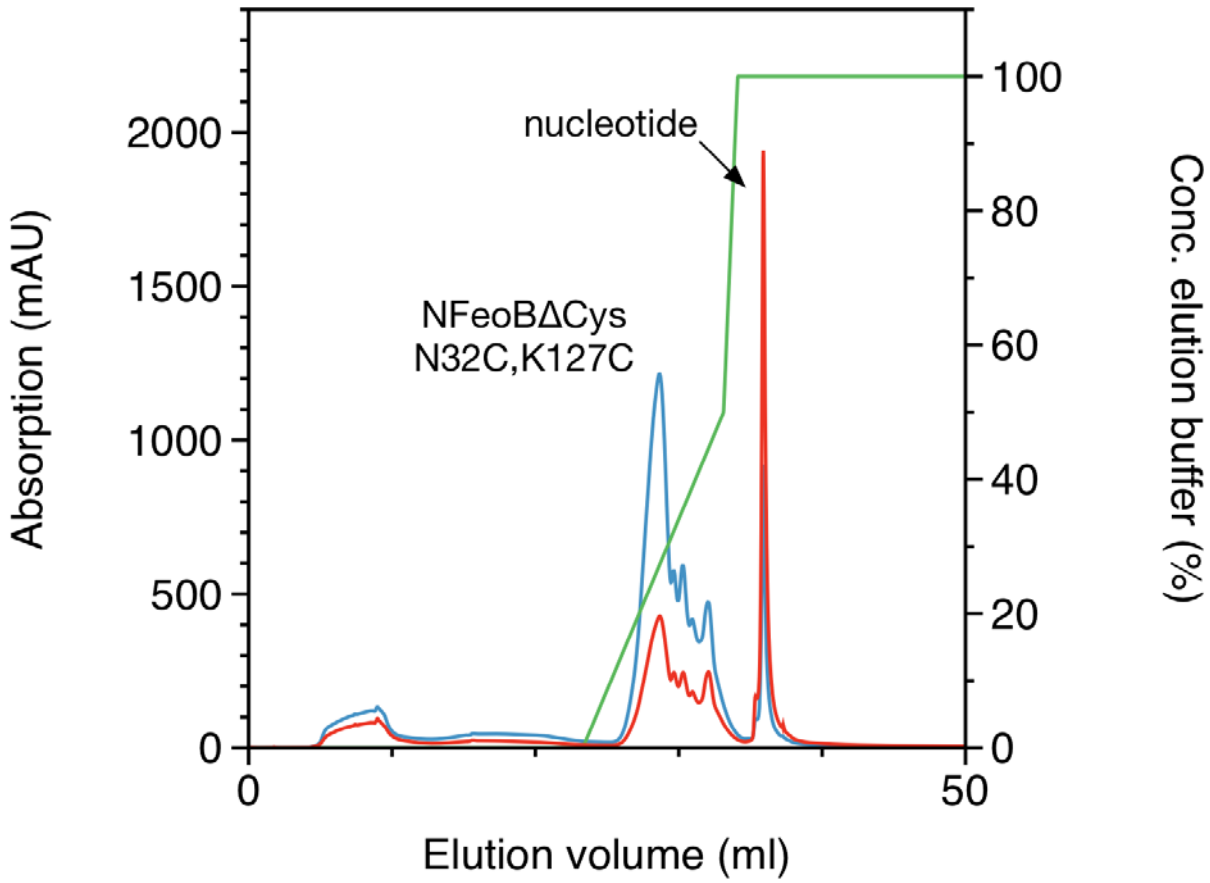

Supplementary Figure 1: Anion exchange chromatography of NFeoBΔCys N32C,K127C. The blue trace shows the absorption at 280 nm and the red trace the absorption at 260 nm. The green line shows the NaCl gradient. The elution buffer contained 1M NaCl, i.e. 100 % elution buffer corresponds to a NaCl concentration of 1M. It is clearly visible that the protein (high absorption at 280 nm) elutes at much lower NaCl concentrations than the copurified nucleotide (GTP or GDP, high absorption at 260 nm).

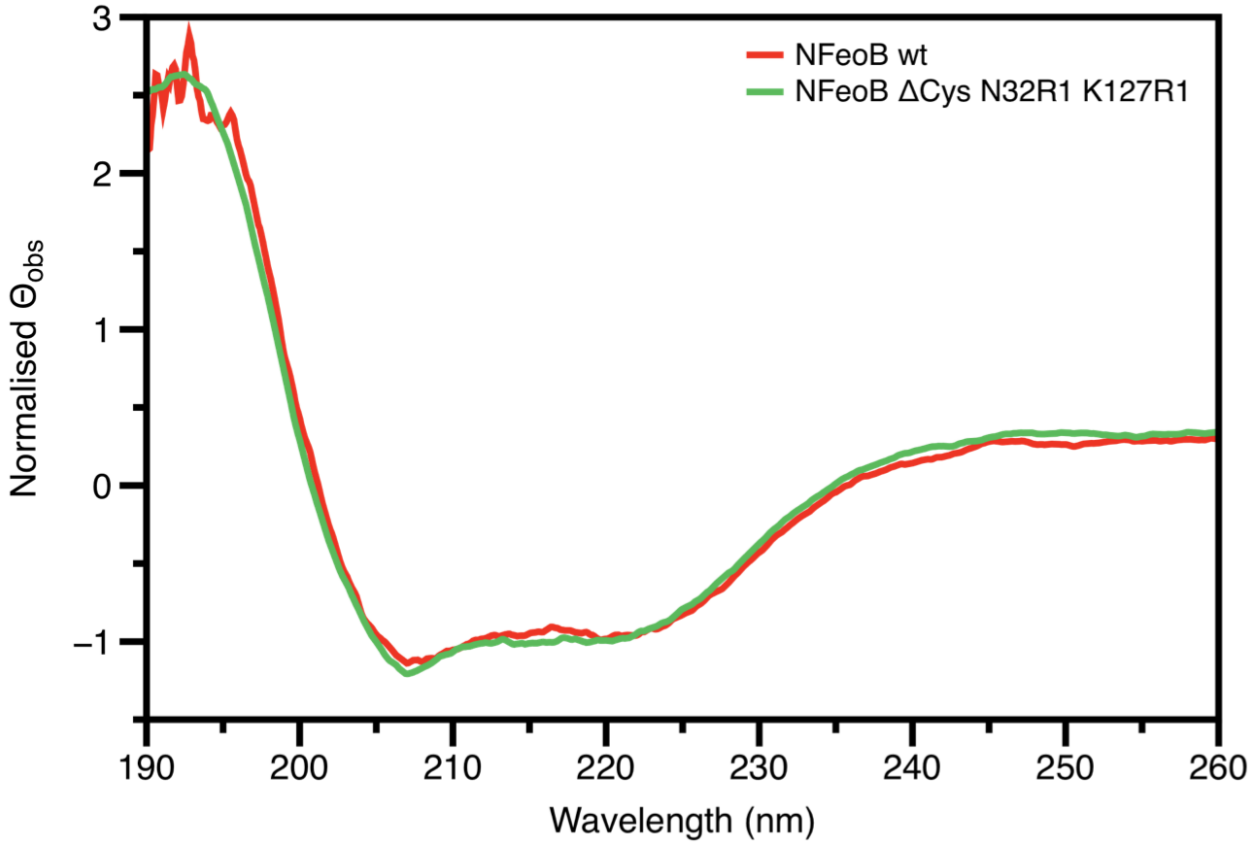

Supplementary Figure 2: Circular dichroism (CD) spectra of NFeoB wt (red) and R1 labelled NFeoB ΔCys N32R1 K127R1 (green).

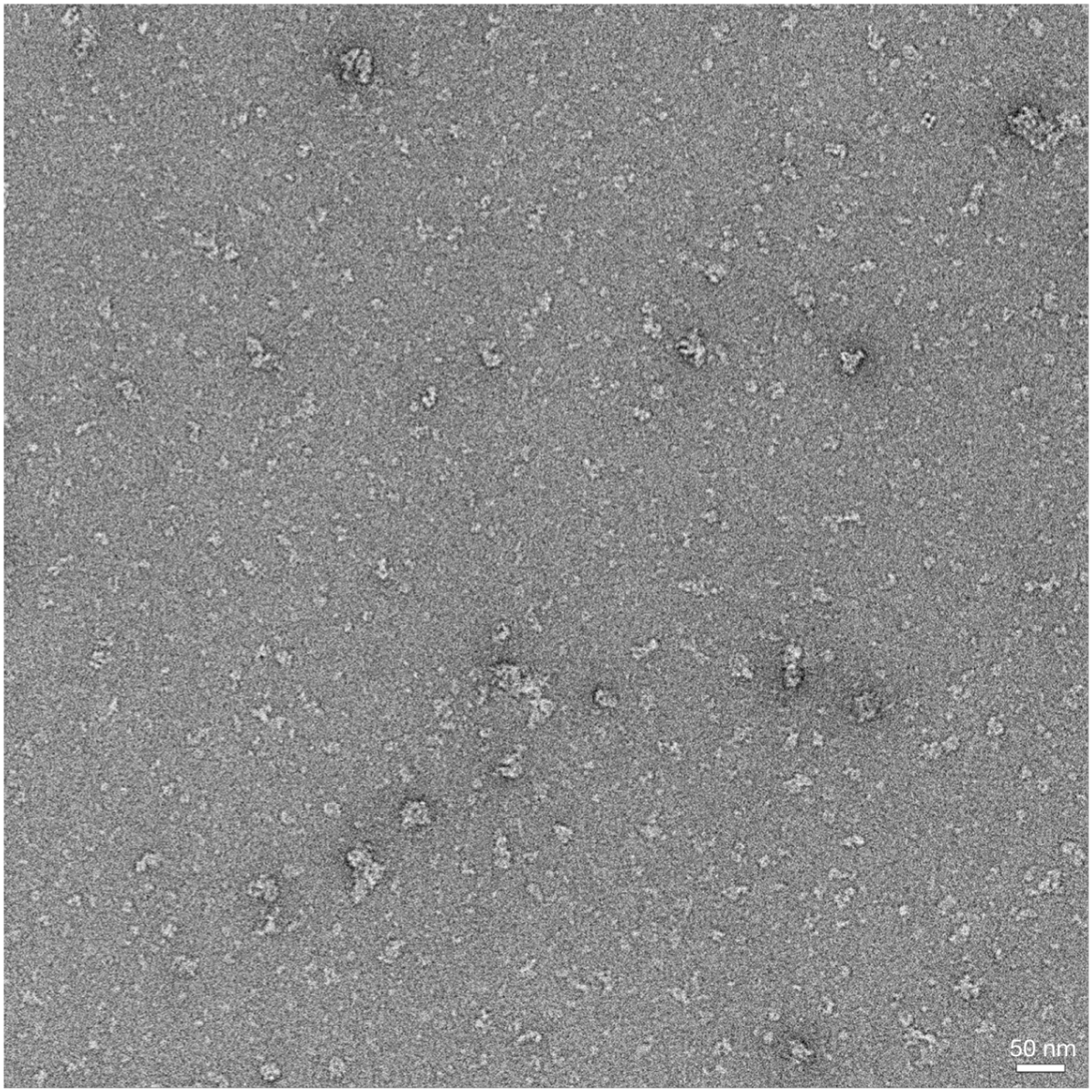

Supplementary Figure 3: Representative negative-stain EM micrograph of DDM solubilised full-length FeoB.

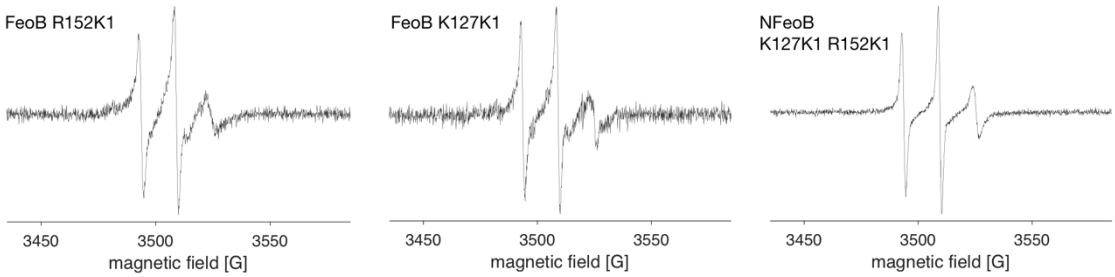

Supplementary Figure 4: Room temperature X-band *cw*-EPR spectra of K1 labelled PELDOR samples.